

Structural Insight into the Interaction between Platelet Integrin $\alpha_{IIb}\beta_3$ and Cytoskeletal Protein Skelemin^{*[5]}

Received for publication, June 6, 2007, and in revised form, August 15, 2007. Published, JBC Papers in Press, September 5, 2007, DOI 10.1074/jbc.M704666200

Lalit Deshmukh[‡], Sergiy Tyukhtenko[‡], Jianmin Liu[§], Joan E. B. Fox[§], Jun Qin[§], and Olga Vinogradova^{‡1}

From the [‡]Department of Pharmaceutical Sciences, School of Pharmacy, University of Connecticut at Storrs, Storrs, Connecticut 06269 and the [§]Department of Molecular Cardiology, Lerner Research Institute, Cleveland Clinic Foundation, Cleveland, Ohio 44195

Skelemin is a large cytoskeletal protein critical for cell morphology. Previous studies have suggested that its two-tandem immunoglobulin C2-like repeats (SkIgC4 and SkIgC5) are involved in binding to integrin β_3 cytoplasmic tail (CT), providing a mechanism for skelemin to regulate integrin-mediated signaling and cell spreading. Using NMR spectroscopy, we have studied the molecular details of the skelemin IgC45 interaction with the cytoplasmic face of integrin $\alpha_{IIb}\beta_3$. Here, we show that skelemin IgC45 domains form a complex not only with integrin β_3 CT but also, surprisingly, with the integrin α_{IIb} CT. Chemical shift mapping experiments demonstrate that both membrane-proximal regions of α_{IIb} and β_3 CTs are involved in binding to skelemin. NMR structural determinations, combined with homology modeling, revealed that SkIgC4 and SkIgC5 both exhibited a conserved Ig-fold and both repeats were required for effective binding to and attenuation of $\alpha_{IIb}\beta_3$ cytoplasmic complex. These data provide the first molecular insight into how skelemin may interact with integrins and regulate integrin-mediated signaling and cell spreading.

The connection between extracellular matrix and the actin cytoskeleton is essential for cell extracellular matrix adhesion. This connection is mediated by a network of protein-protein interactions involving integrins and many cytoskeletal proteins (1, 2). Spatiotemporal regulation of such connection leads to many dynamic cell adhesive processes such as cell shape change (cell spreading), cell migration, and cell survival. Skelemin, a muscle M-line cytoskeletal protein, has been known to play a critical role in mediating the extracellular matrix-actin connection during the early stages of cell spreading by directly interacting with the integrin cytoplasmic face (3–5). Skelemin is a 195-kDa member of a family of cytoskeletal proteins that con-

tains five fibronectin (FN)² type III-like domains and seven immunoglobulin C2-like (IgC) domains (4) (Fig. 1A). Other members of this family, all associated with myosin thick filaments in skeletal and cardiac muscle, include titin (6), twitchin (7), proectin (8), myomesin-II (9), and myosin light-chain kinase (10). Based upon yeast two-hybrid, *in vitro* deletion/competitive binding and *in vivo* transient expression studies, the integrin/skelemin interface was proposed to involve the skelemin IgC domains 4 and 5 (4, 11).

Ig-folds are widely used as scaffolds for protein-protein interactions and are frequently involved in creating networks within the cells as well as bringing adjacent cells together (12). Ig-like domains have been implicated to have versatile binding modes. For example, for titin to complex with telethonin (13), the β -strands from the telethonin Ig-fold align in an anti-parallel arrangement with the last β -strands of the titin Ig-fold, resulting in an Ig-heterotetramer. In case of filamin, Ig-fold bound to the C-terminal part of β integrin cytoplasmic tail (14), the integrin tail forms a β -strand that is aligned anti-parallel to the third and parallel to the fourth β -strand of Ig-fold of filamin on the other side of the β -sandwich. Although skelemin IgC domains 4–5 also bind to integrins, the molecular details for this binding have not been characterized.

In this work, we have undertaken a detailed structural characterization of the skelemin/integrin interaction using NMR as a primary technique. We show that skelemin IgC repeats 4 and 5 exhibit a conserved Ig-fold, and we have characterized their interactions with integrin $\alpha_{IIb}\beta_3$ cytoplasmic tails. Specific regions of contact between the IgC of skelemin and the integrin β_3 CT have been mapped. Our NMR data confirmed that the primary skelemin binding site resides in the membrane proximal region of the β_3 CT (4), while suggesting an additional lower affinity contact within the vicinity of the NPLY motif. Furthermore, surprisingly, we have detected a skelemin binding site in the membrane-proximal region of α_{IIb} CT. Overall, our data provide a molecular template for understanding how SkIgC45 may serve as a modulator of the $\alpha_{IIb}\beta_3$ complex formation and a regulator of integrin clustering.

* The work was supported in parts by National Institutes of Health grants (to J. Q.) and American Heart Association Scientist Development grant (to O. V.). The costs of publication of this article were defrayed in part by the payment of page charges. This article must therefore be hereby marked "advertisement" in accordance with 18 U.S.C. Section 1734 solely to indicate this fact.

[5] The on-line version of this article (available at <http://www.jbc.org>) contains supplemental data, Figs. S6 and S7, and supplemental Table 2.

The atomic coordinates and structure factors (code 2jtd) have been deposited in the Protein Data Bank, Research Collaboratory for Structural Bioinformatics, Rutgers University, New Brunswick, NJ (<http://www.rcsb.org/>).

¹ To whom correspondence should be addressed: Dept. of Pharmaceutical Sciences, 69 North Eagleville Rd., Unit 3092, Storrs, CT 06269-3092, Tel.: 860-486-2972; Fax: 860-486-6857; E-mail: olga.vinogradova@uconn.edu.

² The abbreviations used are: FN, fibronectin; PBS, phosphate-buffered saline; HSQC, heteronuclear single quantum correlation; NOE, nuclear Overhauser effect; NOESY, nuclear Overhauser effect spectroscopy; trNOE, transferred NOE; MBP, maltose-binding protein; CT, cytoplasmic tail; IgC, immunoglobulin C2-like; GST, glutathione S-transferase.

Integrin-Skelemin Interaction



FIGURE 1. **Composition of skelemin.** A, skelemin contains one unique region, one serine/proline-rich region, seven Ig-C2-like and five FN-like domains. SkIgC4 and SkIgC5 domains, *squared* in this figure, have been implicated in integrin binding. B, primary sequences and alignment of skelemin Ig-C2 domains 4 and 5.

EXPERIMENTAL PROCEDURES

Expression and Purification—Cloning, expression, and purification of α_{IIB} CT, β_3 CT, and MBP- β_3 have been described previously (15). The short N-terminal part of the β_3 CT (Lys⁷¹⁶-Trp⁷³⁹; N-terminal part of β_3) was subcloned into pET31b vector (Novagen Inc.) and purified according to the manufacturer's instructions. The short C-terminal part of β_3 CT (Lys⁷³⁸-Thr⁷⁶²; C β_3) was synthesized chemically (Biotechnology Core, Cleveland Clinic Foundation). SkIgC4 (Glu¹²⁰⁷-Phe¹³²⁸), SkIgC5 (Glu¹³³²-Met¹⁴³³) and SkIgC45 (Glu¹²⁰⁷-Met¹⁴³³) were subcloned into pET15b vector (Novagen Inc.) containing an N-terminal His tag using NdeI forward and BamHI reverse cutting sites. SkIgC4 was expressed in BL21(DE3) cells. Rosetta(DE3) cell line from Novagen, expressing rare tRNAs, was employed to improve expression levels of SkIgC5 and SkIgC45. Purification of all skelemin Ig domains was performed according to the protocol from Qiagen under nondenaturing conditions followed by gel filtration on HiLoad 16/60 Superdex 75 column in PBS (140 mM NaCl, 27 mM KCl, 10 mM Na₂HPO₄, 1.8 mM KH₂PO₄, pH 7.4) buffer. To prevent aggregation of SkIgC5, gel filtration was performed in 1% Triton X-100. The aliquot containing an elution peak, corresponding in milliwatt to SkIgC5 dimer, was collected. Using a Millipore Amicon centrifugal 10 kDa filter unit, it was washed thoroughly with 10 volumes of 0.5× PBS and concentrated. GST-fused skelemin domains were purified as described (4). To produce isotopically labeled α_{IIB} CT, β_3 CT, and Sk-IgC4/SkIgC45, cells were grown in M9 minimal medium containing ¹⁵NH₄Cl (1.1 g/liter) and/or ¹³C glucose (3 g/liter) and/or ²H₂O.

NMR Spectroscopy—HSQC (heteronuclear single quantum correlation) titration experiments (summarized in Fig. 2) were performed on 0.1 mM ¹⁵N-labeled β_3 CT or α_{IIB} CT mixed at 1:1, 1:3, 1:5 molar ratios of unlabeled SkIgC4, SkIgC5, and SkIgC45 at 25 °C in 0.25× PBS. Sequence-specific assignments of integrin tails are described elsewhere (15). Transferred NOESY experiments for different peptides were performed at 25 °C in 0.25× PBS with mixing times of 100, 200, 300, and 400 ms to analyze NOE build-up to eliminate spin-diffusion artifacts. Different ratios of the peptides to the binding partner were investigated to find the optimal range for NOE transfer for each particular analysis. The resonance assignments of unlabeled peptides were made using conventional two-dimensional ¹H TOCSY and NOESY spectra (16).

Structure Calculation—All heteronuclear NMR experiments were performed on 1 mM ¹⁵N/¹³C samples of SkIgC4 in 1× PBS adjusted to pH 7.0, and 5% D₂O as described in Clore and Gronenborn (17) on Varian Inova 600 MHz equipped with inverse triple-resonance cryoprobe or Bruker Avance 500 MHz with TXI probe spectrometers. The resonance assignments of double-labeled SkIgC4 were made using standard triple resonance experiments at two temperatures, 25 °C and 40 °C, to resolve the dif-

ferential line-broadening for certain regions of the protein and to overcome degeneracy of peak frequencies. Briefly, HNCACB and HNCA experiments were used for the backbone and H(CC)(CO)HN, (H)CC(CO)HN, and HCCH-TOCSY experiments for side-chain assignments. All the spectra were processed with nmrPipe (18) or TopSpin (Bruker Inc.) and visualized with PIPP (19) or AUREMOL (Bruker Inc.). 2536 NOE distance restraints were obtained from ¹³C- and ¹⁵N-edited three-dimensional NOESY. Dihedral angle restraints were obtained from TALOS (20) and ³J_{H_NH_A}-coupling constants. Structure calculations were performed by CYANA 2.1 (21). Twenty best conformers with lowest target energy functions were subjected to molecular dynamics simulation in explicit water (22) using CNS (23). The protocol for water refinement has been adopted from Jung *et al.* (24). Structures were validated by PROCHECK-NMR (25) and visualized by VMD-XPLOR (26).

RESULTS

Skelemin Binding Site on the Integrin β_3 CT—It has been previously suggested that SkIgC45 binds to integrin β_3 cytoplasmic tail (4). This notion is based on yeast two-hybrid and GST pull-down experiments. To confirm and further characterize this interaction at the molecular level, we performed chemical shift mapping experiments by NMR. Unlabeled SkIgC45 was titrated into the solution of ¹⁵N-labeled β_3 CT, and associated chemical shift perturbations were monitored (Fig. 2A). Chemical shifts changes, plotted as a function of the residue number in β_3 CT (Fig. 2B), clearly show that the membrane-proximal region is most perturbed, confirming that primary binding site resides in this region (4). It should be noted that the extent of the chemical shift perturbations is rather small, which may be because of rapid reversibility and/or low affinity of the interaction. However, the perturbations are reproducible and concentration-dependent. Increase in SkIgC45 to β_3 CT ratio of 5:1 resulted in significant line-broadening and disappearance of some peaks that correspond to the most perturbed N-terminal membrane proximal region of β_3 CT (the Lys⁷¹⁶-Arg⁷²⁴ region; Fig. 2B).

To further characterize the binding interface and to distinguish which of the two Ig domains is essential for this interaction, we titrated unlabeled SkIgC4 and SkIgC5 separately into ¹⁵N-labeled β_3 CT (Fig. 2C). SkIgC5 appears to be primarily

responsible for binding to the membrane-proximal region ending at Asp⁷²³. SkIgC4 causes perturbations mostly around Asn⁷⁴³-Thr⁷⁵⁵. SkIgC45 caused perturbations in both regions albeit in a smaller extent. Interestingly, the Asn⁷⁴³-Thr⁷⁵⁵ binding site overlaps with the filamin Ig domain binding site found in the crystal structure of integrin β_7 in complex with Ig-FLN21 (14) suggesting that SkIgC4 may bind to integrin β_3 tail in a similar manner as filamin. Several additional residues, Ala⁷³⁵, Lys⁷³⁸, and Asp⁷⁴⁰, are also affected by binding to SkIgC4.

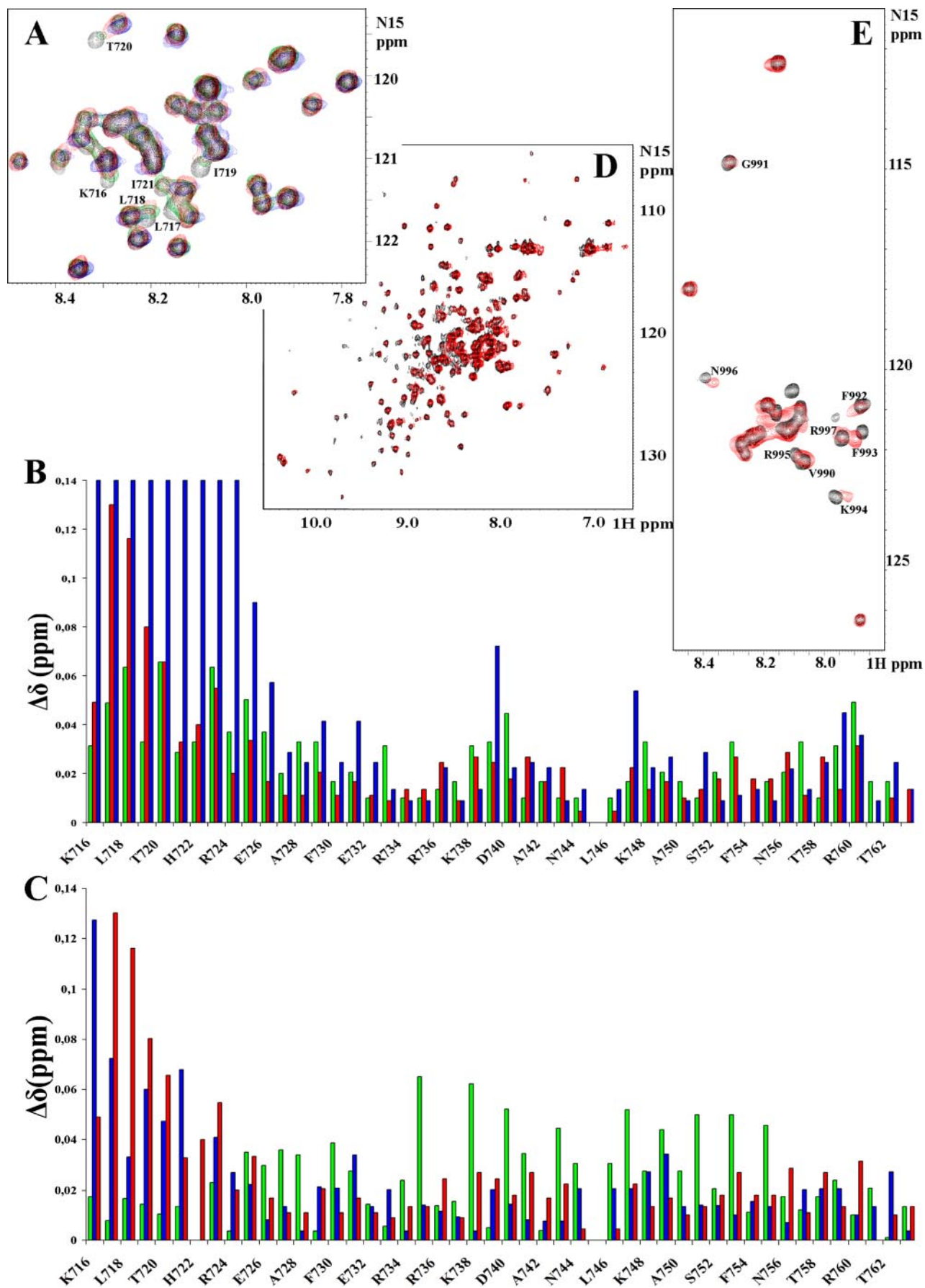
To confirm the above binding data, we employed another method by performing transferred NOE (trNOE) experiments (27). This method is especially well suited to characterize weak interactions (28). Briefly, it is expected that unstructured or only a partially folded peptide assumes a stable conformation upon binding to the target protein, and this process is manifested by appearance of additional peaks in its NOESY spectra. We used short synthetic β_3 peptides composed of either the 24 N-terminal ($N\beta_3$) or 25 C-terminal ($C\beta_3$) residues. IgC4 and IgC5 were fused to glutathione *S*-transferase (GST), respectively, where fusion of GST increased molecular weight of the binding targets to allow favorable NOE transfer (28). $N\beta_3$ mixed with GST-IgC5 exhibited several additional peaks (Fig. 3A, blue, highlighted by arrows) compared with the free unstructured peptide, whereas $N\beta_3$ mixed with GST-IgC4 did not (3A, red). These additional peaks were also observed when $N\beta_3$ was mixed with SkIgC45 (data not shown). In comparison, $C\beta_3$ displayed almost no additional peaks when mixed with GST-IgC5 (Fig. 3B, blue) but exhibited several additional peaks when mixed with GST-IgC4 (3B, red, highlighted by arrows). Interestingly, these peaks are more pronounced and form a slightly different pattern when $C\beta_3$ was mixed with SkIgC45 (Fig. 6 in supplemental data), suggesting that the loop connecting domains 4 and 5 may help to define the proper mutual orientation between integrin β_3 CT and/or tandem skelemin IgC repeats. To conclude, our trNOE data independently validate the above HSQC-based skelemin binding model to integrin β_3 CT, *i.e.* SkIgC5 binds to the N terminus of β_3 CT, whereas SkIgC4 is involved in interaction with C terminus of β_3 CT. The number of additional peaks was limited in both cases, which precluded us from total structure determination of the bound peptides. However, the NOE pattern did suggest that NPLY motif of β_3 forms inverse turn when bound to SkIgC4.

Skelemin Binding Site on the α_{IIB} CT—Having mapped the specific interaction of skelemin with integrin β_3 CT, we performed a control experiment examining whether IgC45 binds to α_{IIB} . To our surprise, the ¹H-¹⁵N HSQC spectrum of α_{IIB} CT also underwent dose-dependent chemical shift changes upon addition of unlabeled SkIgC45 (Fig. 2E). However, no changes were associated with titration of SkIgC4 (data not shown), suggesting that SkIgC5 is a major binding partner for the integrin α_{IIB} subunit. Several peaks, such as the ones corresponding to residues Gly⁹⁹¹, Phe⁹⁹², Lys⁹⁹⁴, and Arg⁹⁹⁷, are significantly broadened and shifted slightly, whereas others, like Val⁹⁹⁰, Phe⁹⁹³, Arg⁹⁹⁵, and Asn⁹⁹⁶, are just shifted. All perturbations are clustered within the membrane-proximal region of α_{IIB} . This is the region involved in the maintenance of the receptor in a latent state by interacting with the membrane-proximal region of β_3 . Interestingly, the most significantly perturbed res-

idues are Phe⁹⁹³, Lys⁹⁹⁴, and Asn⁹⁹⁶, which are located on the opposite side of α_{IIB} interface with β_3 CT (15). This novel finding may have significant impact on our understanding of how skelemin might associate with the integrin cytoplasmic face.

Integrin β_3 Binding Site on Skelemin—We next attempted to investigate the interaction from the skelemin side using the same ¹H-¹⁵N HSQC method. We do see changes in the SkIgC45 spectrum upon addition of full-length β_3 CT, mostly manifested by differential line broadening, but also by some small chemical shifts perturbations (Fig. 2D). However, the overall quality of this spectrum prevents us from making full (or even backbone) resonance assignments of this construct. The molecular weight of SkIgC45 is about 29, which is within modern solution NMR limits, but the protein appears to undergo a significant degree of conformational exchange, and neither deuteration nor TROSY-based experiments at high magnetic field improved the spectral quality. Thus we decided to investigate SkIgC4 and SkIgC5 separately. We found that these two highly similar (about 20% sequence identity, Fig. 1B) domains of skelemin, composing essentially the same fold, behaved very differently in solution. SkIgC4 is a monomer and is characterized by a well dispersed, homogeneous spectrum, which allows not only full resonance assignments but also high-resolution structure determination (see below). However, SkIgC4 ¹H-¹⁵N HSQC spectrum shows no chemical shifts perturbations upon addition of full-length β_3 CT at ratios of up to 1:3 (data not shown). Further increase of this ratio is limited by the insolubility of β_3 CT, which prefers low salt and pH below 6.1, whereas SkIgC4 requires some salt and a pH \sim 7.0 to prevent aggregation. Thus, we again used the short synthetic β_3 peptides, $N\beta_3$ or $C\beta_3$, to examine interactions. We see no changes upon addition of $N\beta_3$ in SkIgC4 ¹H-¹⁵N HSQC spectrum even with high excess of the peptide (ratios of up to 20:1). Very small changes upon addition of $C\beta_3$ in the SkIgC4 ¹H-¹⁵N HSQC spectrum (ratios of up to 40:1) were masked by random changes in frequencies of highly sensitive surface exposed residues, which did not allow us to map unambiguously integrin β_3 binding surface on skelemin IgC4. Addition of α_{IIB} CT has no effect on SkIgC4 HSQC spectrum, confirming the above titration results for ¹⁵N-labeled α_{IIB} subunit. SkIgC5 tends to oligomerize in solution, therefore we do not observe its ¹H-¹⁵N HSQC spectrum because of its slow, on the NMR time scale, tumbling rate. Interestingly, the SkIgC45 construct seemed to behave better than SkIgC5 alone, which allowed us to obtain HSQC despite some conformational exchange problems (Fig. 2D). This finding indicates that SkIgC4 plays an important structural/stabilizing role in the solution behavior of SkIgC45.

NMR Structure of SkIgC4 and Homology Modeling of SkIgC5—To verify fold and characterize unique features of skelemin IgC domains 4 and 5, we performed detailed structural analysis. First, we determined the high-resolution structure of SkIgC4 by modern triple resonance NMR methods as described in the “Structure Calculation” section of the “Experimental Procedures” (assignments are presented in Table 2 of supplemental data). As expected, SkIgC4 adopts a very well known Ig-fold and contains seven β -strands in two β -sheets, which form a β -sandwich. Apart from these β -strands, however, SkIgC4 contains unique features, namely two alpha heli-



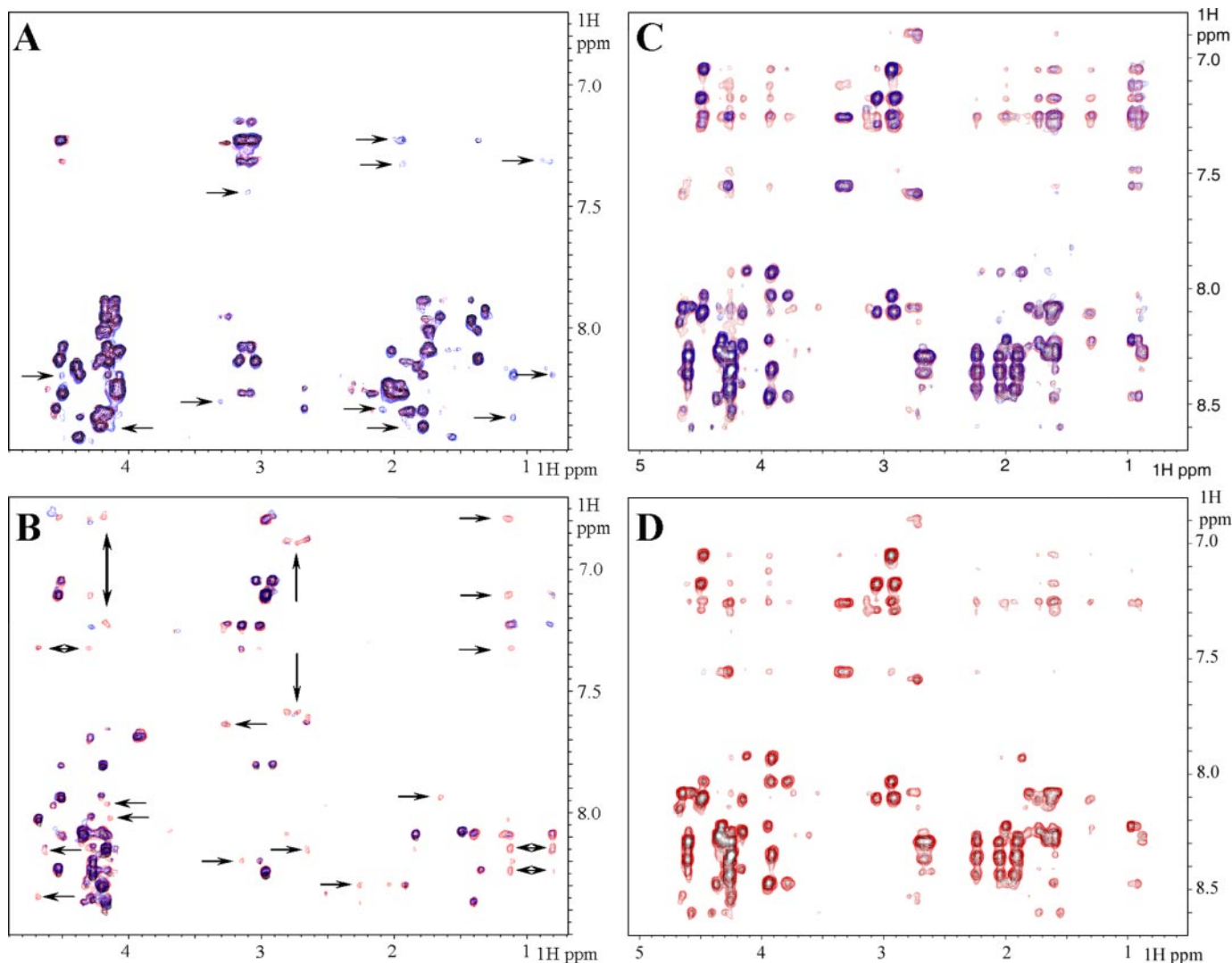


FIGURE 3. Transferred NOEs evidence for integrin β_3 /skelemin and α_{IIb} /skelemin interactions. All shown trNOE experiments were performed at 25 °C (400 ms mixing time) in 0.25× PBS buffer (pH 6.2; 5 mM Ca^{2+} was added to the samples used for experiments presented in panels C and D to stabilize α_{IIb} CT as described earlier (15, 32)). Superposition of NOESY spectra are presented as follows: A, β_3 alone (black) and in complex with skelemin GST-IgC5 (blue, some additional peaks are highlighted by arrows) or with GST-IgC4 (red) at the ratios of 20:1; B, β_3 alone (black) and in complex with skelemin GST-IgC5 (blue) or with GST-IgC4 (red, some additional peaks are highlighted by arrows) at the ratios of 20:1; C, α_{IIb} alone (black), in the presence of MBP- β_3 (red) at the ratio of 100:1 showing additional peaks, a manifestation of trNOE effect reported previously (15) and in the presence of both MBP- β_3 and SklgC45 (blue) at the ratio of 100:1:3, showing reduced number of attenuated additional peaks; D, α_{IIb} alone (black) and in the presence of SklgC45 (red) at the ratio 100:1, showing additional peaks, but the pattern is somewhat different from the one seen in C.

ces, referred to as N-terminal H1 and C-terminal H2. Fig. 4A maps SklgC4 secondary structural elements, and 4B shows a schematic representation of their arrangement. In accordance with the IgC-fold, β -strands A, B, E, and F form one face of the β -sandwich and strands C, F, and G form the other face (Fig. 4C). Interestingly, there is one short β -strand (D'), which runs almost perpendicular to strand C. This feature is not observed

often in IgC-folds. The N-terminal H1 is made up of six amino acid residues and is followed by a long flexible region (13 residues), which connects it to β -strand A. The C-terminal H2 is composed of 10 residues and is attached to β -strand G by a short loop. Additionally, there is a helix-like turn, which connects β -strands E and F. Fig. 4D presents the backbone superposition of 20 calculated structures with the lowest target

FIGURE 2. Summary of the spectral perturbations for integrin β_3 /skelemin and α_{IIb} /skelemin interactions. All experiments were performed in 0.25× PBS (pH 6.2) buffer at 25 °C. A, expanded region of HSQC spectra of ^{15}N -labeled β_3 tail in the absence (black) and presence of the unlabeled skelemin IgC45 at different ratios: 1:1, green; 1:3, red; 1:5, blue. Residues labeled indicate the most significant changes. B, chemical shift changes of the β_3 tail upon SklgC45 binding. Bars are colored according to the different ratios as presented in A. First nine residues (Lys 716 -Arg 724) in 1:5 (blue) series are undetectable because of extreme line-broadening and are shown as bars with maximum values. C, chemical shift changes of the β_3 tail upon binding to different skelemin constructs at the ratio of 1:3. Bars are colored according to the interaction with a particular domain of skelemin: green bars, interaction with SklgC4; blue bars, interaction with SklgC5; red bars, interaction with SklgC45. The last bar in each series represents chemical shifts of the Trp 739 side-chain HN; His 722 is undetectable (probably because of the exchange with water) and is not shown in green and blue series. $\Delta\delta(\text{HN},\text{N})$ in ppm refers to the combined HN and N chemical shift changes, according to the equation: $\Delta\delta(\text{HN},\text{N}) = ((\Delta\delta_{\text{HN}})^2 + 0.2(\Delta\delta_{\text{N}})^2)^{1/2}$, where $\Delta\delta = \delta_{\text{bound}} - \delta_{\text{free}}$. D, HSQC spectra of $^{15}\text{N}/^2\text{H}$ -labeled skelemin IgC45 in the absence (black) and presence (red) of the unlabeled β_3 tail. E, HSQC spectra of ^{15}N -labeled α_{IIb} in the absence (black) or presence (red) of unlabeled SklgC45 at the ratio of 1:5.

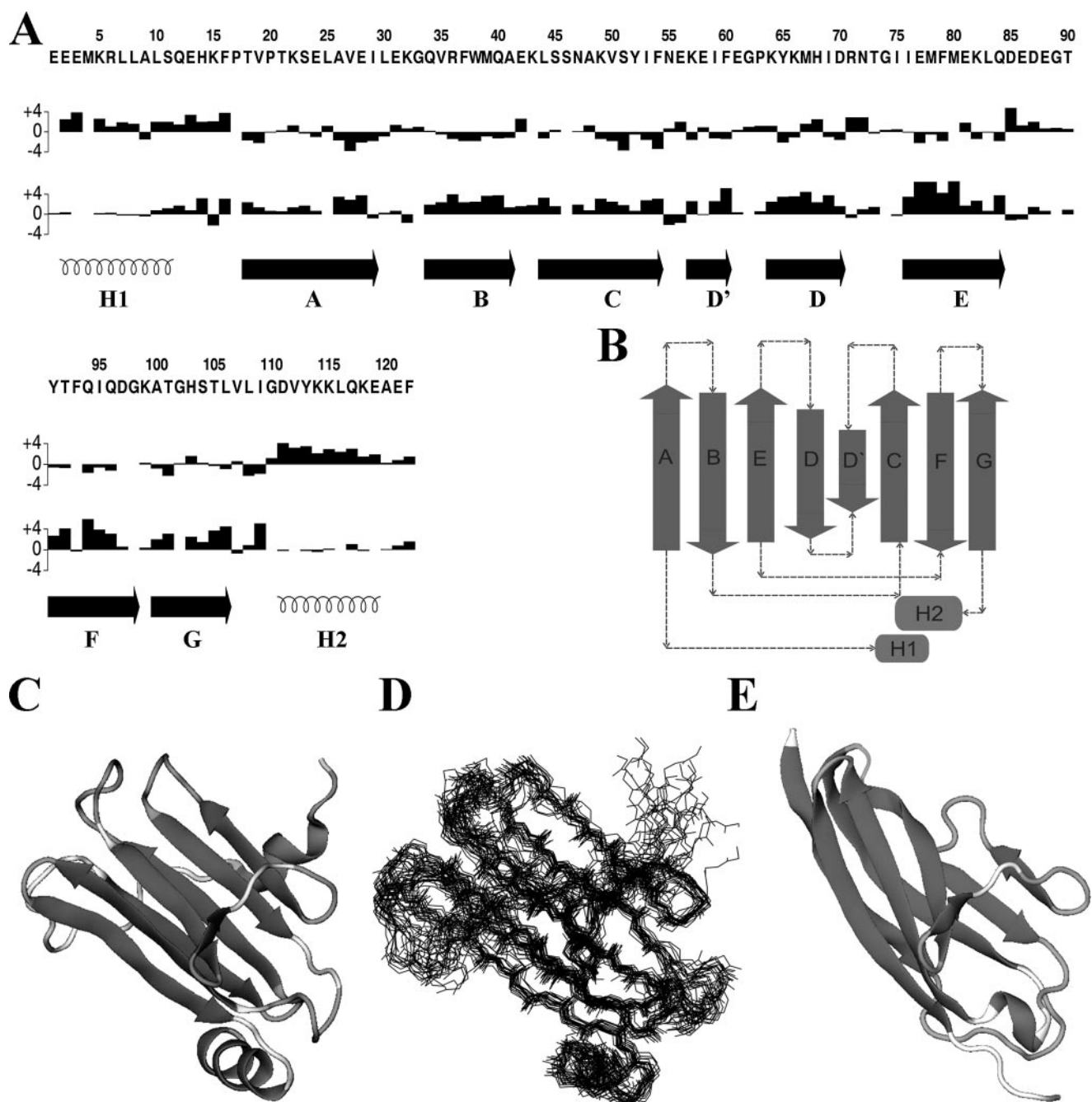


FIGURE 4. Structure of SkIgC4 and model of SkIgC5 domains. *A*, secondary structure elements of skelemin IgC4 calculated from the differences between $^{13}\text{C}_\alpha$ and $^{13}\text{C}_\beta$ shifts for each residue and corresponding random coil value. *B*, arrangement of those secondary structure elements according to Ig-C2-fold. *C*, backbone ribbon diagram of SkIgC4. The figure was generated by VMD-XPLOR (26). *D*, backbone superposition of the 20 best structures of SkIgC4 presented from the same point of view as *panel C*. *E*, model of SkIgC5 built by three-dimensional JIGSAW program (29).

energy functions. This ensemble has been deposited to Protein Data Bank (access code 2jtd). Statistics of this ensemble are presented in Table 1 demonstrate a very high quality structure (see also Ramachandran plot, Fig. 7 in supplemental data).

The poor behavior of SkIgC5 in solution precludes its detailed structure determination by NMR. We, therefore, used the three-dimensional JIGSAW program (29) to build a three-dimensional model for SkIgC5 (Fig. 4*E*) based on the homology to known structures, NCAM Ig-3 (12) and titin Ig-Z2 (13). As expected, it also adopts well defined Ig-C2-fold.

Influence of Skelemin on the Integrin $\alpha_{\text{IIb}}\beta_3$ Cytoplasmic Complex and Its Implication on Integrin Signaling—The CTs of α_{IIb} and β_3 form a clasp to maintain the integrin in an inactive conformation, and talin can activate the integrin by unclamping this complex (reviewed in Ref. 30). Our discovery that skelemin can bind to both α_{IIb} and β_3 CTs has prompted us to investigate its influence on the CT complex. To find out if skelemin disrupts this clasp, we applied the same approach we used previously for studying integrin/talin interactions (15). In the case of talin/integrin interaction, talin competes with the α_{IIb} CT for binding to the β_3 CT fused to MBP (MBP- β_3 CT) and abolished

TABLE 1
Structural statistics of skelemin IgC4 domain

Parameter	Ensemble ^a
Distance restraints	
All	2536
Short range ($ i - j \leq 1$)	1807
Medium range ($1 < i - j < 5$)	190
Long range ($ i - j \geq 5$)	539
Dihedral angle restraints^b	
	157
Hydrogen bond restraints^c	
	14
Violations	
NOE ($>0.5 \text{ \AA}$)	0
Dihedrals ($>5^\circ$)	0
Average CYANA target function value^d	
	2.30
r.m.s.d.^e (residues 20–110)	
Average backbone r.m.s.d. mean	0.63 ± 0.12^f 0.94 ± 0.09^g
Average heavy atom r.m.s.d. to mean	1.07 ± 0.12^f 1.38 ± 0.11^g
VanderWaal energy	
	-489.1 ± 22.7
Ramchandran plot^h	
Residues in most favored regions	83.3%
Residues in additional allowed regions	16.6%
Residues in generously allowed regions	0.1%
Residues in disallowed regions	0%
r.m.s.d. from idealized covalent geometry	
Bonds (\AA)	0.0034 ± 0.0001
Angles ($^\circ$)	0.502 ± 0.018
Impropers ($^\circ$)	1.518 ± 0.140

^a Mean \pm S.E. where applicable.

^b Generated from TALOS (20) and j-HNHA.

^c Hydrogen bonds were included at the last stage of structure calculation.

^d Average target function value before energy minimization.

^e r.m.s.d., root mean square deviation.

^f r.m.s.d. calculated by CYANA before water refinement. Residues 1–19 and 111–122 were excluded due to the dynamic disorder in these regions.

^g r.m.s.d. for the same residues calculated after water refinement.

^h Calculated by PROCHECK_NMR (25).

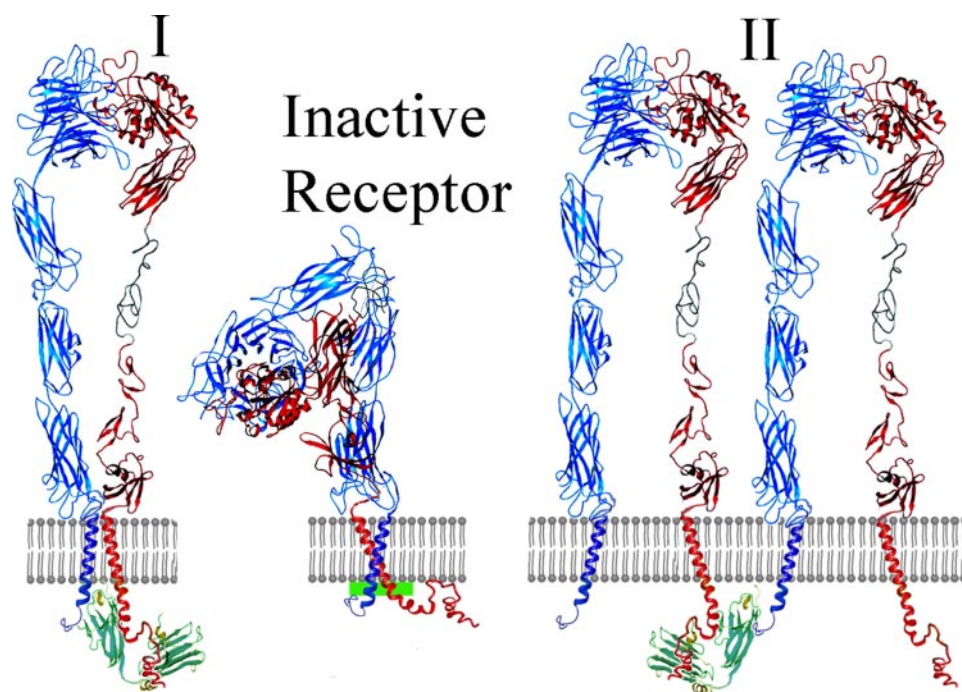


FIGURE 5. Model of $\alpha_{IIB}\beta_3$ /skelemin tertiary complex. Skelemin interaction with integrin cytoplasmic complex might initiate and/or stabilize receptor activation in two possible ways. *I*, skelemin may disrupt the $\alpha_{IIB}\beta_3$ cytoplasmic complex but keep α_{IIB} and β_3 CTs in close proximity by sitting in between and binding to both subunits. *II*, skelemin may bind to the individual α_{IIB} and β_3 CTs from two different heterodimers, thus separating $\alpha\beta$ intraclass while connecting two adjacent receptors. Tendency of SklgC5 domain to oligomerize further stimulates and stabilizes integrins cluster formation by promoting both homo- and hetero-oligomerization.

the trNOE induced by the α_{IIB} CT. However, when we added SklgC45 to α_{IIB} CT/MBP- β_3 CT mixture (Fig. 3C), we saw attenuation but not total elimination of the trNOE peaks. Some trNOE peaks do disappear but many remain. Because the α_{IIB} CT also binds to SklgC45, some of the trNOE peaks could arise from this interaction. Indeed, when we added SklgC45 into free α_{IIB} , we saw a number of trNOE (Fig. 3D). The additional peaks observed are consistent with our HSQC binding data (Fig. 2C) implicating the membrane-proximal region of the α_{IIB} CT in the interaction. However, this latter spectral pattern is different from one of the α_{IIB} CT in the presence of both MBP- β_3 CT and SklgC45 (Fig. 3C). This observation suggests that SklgC45 attenuates the $\alpha_{IIB}\beta_3$ CT clasp; however, complexity of the system and limits of the experimental approach do not allow us to conclude that this complex is fully disrupted by skelemin.

DISCUSSION

In this study, we have performed detailed NMR experiments to understand the nature of the skelemin/integrin interaction. Our data not only confirm skelemin IgC45 interaction with integrin β_3 CT but also show for the first time that it binds to integrin α_{IIB} CT. Detailed chemical shift mapping and transferred NOE analysis allowed us to pinpoint the specific regions within both α_{IIB} and β_3 CTs involved in interaction with skelemin. In particular, our studies revealed that the membrane proximal regions of both the α_{IIB} and β_3 CT are involved in binding to skelemin. The structural analysis demonstrates that skelemin IgC repeats 4 and 5 do adopt canonical Ig-folds but recognize the integrin in different ways. SklgC4 appears to interact weakly with C terminus of β_3 CT, whereas SklgC5 binds to both N-terminal membrane-proximal regions of α_{IIB} and β_3 CTs.

Whether skelemin interacts with $\alpha_{IIB}\beta_3$ before or after integrin activation remains unknown although skelemin has been shown to be critical for cell spreading (an outside-in signaling event) suggesting that skelemin is at least involved in binding to integrin after integrin activation. Our NMR data suggest that skelemin exerts a different effect on the structure of the $\alpha_{IIB}\beta_3$ CT complex as compared with talin. Although the final conclusion awaits the structure determination of skelemin/integrin complex, the transferred NOE and the HSQC binding data suggest two major possibilities (Fig. 5). Skelemin may disrupt the $\alpha_{IIB}\beta_3$ cytoplasmic complex but may sit in between α_{IIB} and β_3 CTs by binding to both subunits (Fig. 5, *I*). Skelemin may bind to the individual α_{IIB} and β_3 CTs

from two different heterodimers, thus separating $\alpha\beta$ intracasp while connecting two adjacent receptors (Fig. 5, II). The first possibility is consistent with noticeable attenuation of trNOEs in $\alpha_{IIb}\beta_3$ CT complex upon addition of SkIgC45 (Fig. 3C). The latter option is consistent with the HSQC data on SkIgC45/ α_{IIb} interaction (Fig. 2D) where skelemin binding to α_{IIb} CT affects mostly residues of the membrane-proximal region, which are not directly involved in the α_{IIb}/β_3 CT interface. These residues are Phe⁹⁹³, Lys⁹⁹⁴, and Asn⁹⁹⁶, and they are located on the opposite side of α_{IIb} interface with β_3 CT. Nevertheless, because skelemin is involved in the formation of the nascent focal adhesions regulating the cytoskeleton organization, both possibilities may enhance integrin clustering, which is essential for cell spreading, a major finding as to how skelemin regulates integrin signaling (11). If skelemin is recruited to the inactive integrin, it may contribute to the receptor activation in certain cell types because it does have some weak unclasp activity (possibility I). The unclasp event could be further enhanced by other integrin activators such as talin. In possibility II, skelemin may stabilize the activated state of integrin by promoting clustering via a hetero-oligomerization mechanism. Furthermore, both the α_{IIb} and β_3 transmembrane plus cytoplasmic domains are shown to form homooligomers (31). Considering the strong tendency of SkIgC5 to oligomerize as well, IgC5 domains from two different skelemin molecules could form a dimer, bridging two adjacent integrin homo-subunits. Thus skelemin may play an important role in the stabilization of integrin clusters by promoting both homo- and hetero- oligomerization.

To conclude, we have (i) defined for the first time skelemin binding surface on platelet integrin $\alpha_{IIb}\beta_3$, which involves both hetero-subunits; (ii) demonstrated that this interaction attenuates the inter-subunit clasp, found in inactivated state of the receptor; and (iii) structurally characterized skelemin tandem Ig-C2-like repeats 4 and 5 and showed that the two repeats contributed to integrin binding in a different but cooperative manner. Based upon these data, we propose that skelemin regulates integrin cluster formation at earlier stages of cell spreading. This model should help to design new experiments to better understand its mechanism of action.

Acknowledgments—We thank Frank Delaglio and Dan Garrett for NMR software, Kumar Reddy for skelemin cDNA, and Ed Plow for stimulating discussions.

REFERENCES

- Hynes, R. O. (1992) *Cell* **69**, 11–25
- Schwartz, M. A., Schaller, M. D., and Ginsberg, M. H. (1995) *Annu. Rev. Cell Dev. Biol.* **11**, 549–599
- Price, M. G., and Gomer, R. H. (1993) *J. Biol. Chem.* **268**, 21800–21810
- Reddy, K. B., Gascard, P., Price, M. G., Negrescu, E. V., and Fox, J. E. (1998) *J. Biol. Chem.* **273**, 35039–35047
- Steiner, F., Weber, K., and Furst, D. O. (1999) *Genomics* **56**, 78–89
- Labeit, S., Barlow, D. P., Gautel, M., Gibson, T., Holt, J., Hsieh, C. L., Francke, U., Leonard, K., Wardale, J., Whiting, A., et al. (1990) *Nature* **345**, 273–276
- Benian, G. M., Kiff, J. E., Neckelmann, N., Moerman, D. G., and Waterston, R. H. (1989) *Nature* **342**, 45–50
- Ayme-Southgate, A., Vigoreaux, J., Benian, G., and Pardue, M. L. (1991) *Proc. Natl. Acad. Sci. U. S. A.* **88**, 7973–7977
- Noguchi, J., Yanagisawa, M., Imamura, M., Kasuya, Y., Sakurai, T., Tanaka, T., and Masaki, T. (1992) *J. Biol. Chem.* **267**, 20302–20310
- Olson, N. J., Pearson, R. B., Needleman, D. S., Hurwitz, M. Y., Kemp, B. E., and Means, A. R. (1990) *Proc. Natl. Acad. Sci. U. S. A.* **87**, 2284–2288
- Reddy, K. B., Bialkowska, K., and Fox, J. E. (2001) *J. Biol. Chem.* **276**, 28300–28308
- Soroka, V., Kolkova, K., Kastrup, J. S., Diederichs, K., Breed, J., Kiselyov, V. V., Poulsen, F. M., Larsen, I. K., Welte, W., Berezin, V., Bock, E., and Kasper, C. (2003) *Structure* **11**, 1291–1301
- Zou, P., Pinotsis, N., Lange, S., Song, Y. H., Popov, A., Mavridis, I., Mayans, O. M., Gautel, M., and Wilmanns, M. (2006) *Nature* **439**, 229–233
- Kiema, T., Lad, Y., Jiang, P., Oxley, C. L., Baldassarre, M., Wegener, K. L., Campbell, I. D., Ylanne, J., and Calderwood, D. A. (2006) *Mol. Cell* **21**, 337–347
- Vinogradova, O., Velyvis, A., Velyviene, A., Hu, B., Haas, T., Plow, E., and Qin, J. (2002) *Cell* **110**, 587–597
- Wuthrich, K. (1986) *NMR of proteins and nucleic acids*, John Wiley & Sons, New York
- Clore, G. M., and Gronenborn, A. M. (1998) *Curr. Opin. Chem. Biol.* **2**, 564–570
- Delaglio, F., Grzesiek, S., Vuister, G. W., Zhu, G., Pfeifer, J., and Bax, A. (1995) *J. Biomol. NMR* **6**, 277–293
- Garrett, D. S., Powers, R., Gronenborn, A. M., and Clore, G. M. (1991) *J. of Magn. Reson.* **95**, 214–220
- Cornilescu, G., Delaglio, F., and Bax, A. (1999) *J. Biomol. NMR* **13**, 289–302
- Guntert, P. (2004) *Methods Mol. Biol.* **278**, 353–378
- Linge, J. P., Williams, M. A., Spronk, C. A., Bonvin, A. M., and Nilges, M. (2003) *Proteins* **50**, 496–506
- Brunger, A. T., Adams, P. D., Clore, G. M., DeLano, W. L., Gros, P., Grosse-Kunstleve, R. W., Jiang, J. S., Kuszewski, J., Nilges, M., Pannu, N. S., Read, R. J., Rice, L. M., Simonson, T., and Warren, G. L. (1998) *Acta Crystallogr. Sect. D Biol. Crystallogr.* **54**, 905–921
- Jung, J. W., Yee, A., Wu, B., Arrowsmith, C. H., and Lee, W. (2005) *J. Biochem. Mol. Biol.* **38**, 550–554
- Laskowski, R. A., MacArthur, M., Moss, D. S., and Thornton, J. M. (1993) *J. Appl. Crystallogr.* **26**, 283–291
- Schwieters, C. D., and Clore, G. M. (2001) *J. Magn. Reson.* **149**, 239–244
- Clore, G. M., and Gronenborn, A. M. (1982) *J. Magn. Reson.* **48**, 402–417
- Vaynberg, J., and Qin, J. (2006) *Trends Biotechnol.* **24**, 22–27
- Bates, P. A., Kelley, L. A., MacCallum, R. M., and Sternberg, M. J. (2001) *Proteins* **5**, (suppl.) 39–46
- Hynes, R. O. (2002) *Cell* **110**, 673–687
- Li, R., Babu, C. R., Lear, J. D., Wand, A. J., Bennett, J. S., and DeGrado, W. F. (2001) *Proc. Natl. Acad. Sci. U. S. A.* **98**, 12462–12467
- Vinogradova, O., Haas, T., Plow, E. F., and Qin, J. (2000) *Proc. Natl. Acad. Sci. U. S. A.* **97**, 1450–1455